JOURNAL OF COMPUTATIONAL PHYSICS 12, 348–363 (1973)

Numerical Study of Viscous Flow in a Cavity*

JAMES D. BOZEMAN

The Offshore Company, Houston, Texas

AND

CHARLES DALTON

Department of Mechanical Engineering, University of Houston, Houston, Texas

Received August 28, 1972

Numerical solutions have been obtained for the steady two-dimensional flow of a viscous incompressible fluid in rectangular cavities by solving various implicit finite-difference approximations of the Navier–Stokes equations. The sets of implicit difference equations were solved using a recently introduced iterative numerical scheme called the strongly implicit procedure. The strongly implicit procedure was found to be an effective and economical numerical scheme for obtaining iterative solutions for sets of linear finite-difference equations. Various qualitative and quantitative comparisons have been made to determine the effects of Reynolds number and grid size on four different finite-difference forms of the governing equations. The results show that one difference scheme was particularly accurate for Reynolds numbers and grid sizes which satisfy the Thom and Apelt stability restriction. Streamline plots for Reynolds numbers of 100 and 1000 are shown. The behavior of the vortex center and secondary vortices with increasing Reynolds number is exhibited. The growth of the secondary vortices with increasing cavity depth is also shown.

1. INTRODUCTION

The fluid motion generated in a rectangular cavity by the uniform translation of the upper surface of the cavity is an example of a closed streamline problem. We consider this physical problem from the viewpoint of obtaining numerical solutions to the Navier–Stokes equations to describe the fluid motion.

The cavity problem is of theoretical importance because it is a part of the larger class of steady separated flows which are reviewed and discussed in detail by Burggraf [1]. The features of the cavity flow are well known and others (Pan and

* Based on the dissertation of JDB as submitted to the University of Houston, 1972.

Copyright © 1973 by Academc Press, Inc.
All rights of reproduction in any form reserved.

Acrivos [2]; Greenspan [3]; Runchal, Spalding, and Wolfshtein [4]; Kawaguti [5]) besides Burggraf have sought accurate numerical solutions to this problem over a range of Reynolds numbers defined as $R = Vd/\nu$, where V is the velocity of the top plate, d is the width of the cavity and ν is the kinematic viscosity. The characteristics of the flow are as follows: The nature of the vortex formed in the cavity depends on the aspect ratio (cavity height to width ratio) as well as the Reynolds number. For an aspect ratio of unity and relatively low Reynolds numbers, the center of the vortex is located about three-quarters of the cavity height from the bottom and at midwidth. Most of the strength of the vortex is concentrated in the upper portion of the cavity. There are a pair of small counterrotating vortices of much smaller strength located in the lower corners of the cavity. As the Reynolds number increases, the vortex center moves downstream. With further increases in Reynolds number, the vortex center moves down and toward the center of the cavity (see Fig. 4). Also, as the Reynolds number increases, the calculated value of the vorticity becomes approximately uniform over the center of the vortex. A model proposed by Batchelor [6] is of importance in interpretation of the calculated results. Batchelor proposed that the limiting laminar flow case ($\nu \to 0$) consists of a recirculating eddy having uniform vorticity over an inviscid core with viscous effects confined to the infinitesimally thin shear layers along the boundaries.

For aspect ratios greater than one, the number of vortices in the cavity depends on the value of the aspect ratio. Visual studies by Mills [7] and Pan and Acrivos [2] have indicated the behavior of the vortex pattern for different aspect ratios. The downstream corner vortex becomes larger with increasing aspect ratio. At an aspect ratio of two, the downstream corner vortex has grown until it occupies the entire lower portion of the cavity. The relative position of the pair of vortices depends on the Reynolds number. For an infinitely deep cavity, a series of vortices is generated. Since the vortex strength decreases sharply as the depth into the cavity is increased, not all of the vortices may be observed. Pan and Acrivos show the first three of the vortices at a Reynolds number of 3200. The remaining vortices are too weak to be observed at this Reynolds number. The development of the vortex pattern as the aspect ratio increases is not well understood in spite of the flow visualization studies of Pan and Acrivos and of Mills.

The cavity-flow problem is of continuing interest because it offers a relatively simple model on which numerical techniques may examined. One of the main problems in doing numerical fluid mechanics is that the grid size must decrease as the Reynolds number increases so that numerical stability is obtained. Therefore, improvements and tradeoffs in the convergence criterion may be studied with relative ease using this model. Furthermore, previous investigators have left certain gaps in the understanding of the flow field. These gaps, and sometimes discrepancies, will be discussed as the development and comparisons are made.

2. Summary of Other Investigations

Burggraf [1] did an extensive numerical study on the cavity-flow problem using a modified relaxation method. His calculations were for a square cavity in the Reynolds number range from 0 to 400 with mesh spacings from 1/10 to 1/40. The motion of the vortex center toward the center of the cavity, as the Reynolds number increases, is demonstrated. Burggraf also examined the behavior of the secondary vortices in the lower corners of the cavity. He noted that the secondary vortex pattern was viscosity-dominated in contrast with the relatively nonviscous primary eddy.

Using the same relaxation scheme as Burggraf, Pan and Acrivos [2] obtained detailed numerical solutions to the problem of creeping flow in a cavity. The primary vortex at a Reynolds number of zero was found to be symmetrical for all cavity depths considered. They found a sequence of counterrotating vortices of decreasing strength and size in the immediate vicinity of the corner. The method of Moffatt [8] was used to calculate the corner vortices since these seemed not to influence the primary vortex once a converged solution had been obtained for it. Since Bruggraf had experienced numerical instabilities for $R > 400$, Pan and Acrivos did not attempt to extend their numerical solutions past the creeping flow problem.

Pan and Acrivos also conducted a flow-visualization study of the cavity–flow behavior over a wide range of Reynolds numbers which for a square cavity went from 80 to 4000. The visualization studies produced flow fields consistent with the model of Batchelor [6]. The value of 4000 was the Reynolds number at which flow instability had begun to appear.

Mills [7] examined the cavity problem at a Reynolds number of 100 at aspect ratios of 0.5, 1, and 2. Mills used central differences and applied Liebmann's iterative technique to obtain his solution. The mesh system used was one in which the lines connecting the mesh points varied in the same ratio as the aspect ratio of the cavity. The convergence criterion of Thom and Apelt [9],

$$(h/d) < 40^{1/2}/R,$$

was used by Mills in his study and resulted in a horizontal mesh spacing of $d/14$.

Mills conducted flow-visualization studies of the three aspect ratios which he also examined numerically. He noted good agreement in all three cases except that the corner vortices were not observed in the visualization studies.

Greenspan [3, 10] considered the cavity-flow problem numerically by means of the generalized Newton's method with overrelaxation. Greenspan was able to obtain solutions at Reynolds numbers of 200, 500, 2000, and 15,000 for a mesh spacing of 1/20. For a mesh spacing of 1/40, Greenspan determined solutions at Reynolds numbers of 50, 10^4, and 10^5.

Greenspan's convergence criteria involved differences between successive iterates of both the stream function and the vorticity. Use of this kind of criteria does not necessarily specify convergence; it simply generates solutions which do not change appreciably with further iterations. Greenspan did not notice any secondary vortices for a mesh spacing of 1/20 for any of the Reynolds numbers for which he made calculations. The secondary vortices should have been detectable at this mesh spacing as they were found by Pan and Acrivos to be sufficiently large. In fact, the present study has determined the presence of the secondary vortices at this mesh spacing.

Another set of studies relating to the cavity flow problem was by Runchal, Spalding and Wolfshtein [4], Runchal and Wolfshtein [11] and Gosman et al. [12]. This series of studies, all conducted by the Imperial College at London group, had two features not present in the previous investigations. One feature involved the use of a nonuniform mesh system to improve the accuracy of the solution. The other feature involved an evaluation of the wall vorticity which was an improvement over that used by previous investigators.

The Imperial College group used an unidirectional differencing technique on vorticity gradients in such a way that the differencing was always backwards with reference to the direction of flow. The unidirectional differencing procedure allowed both the convergence criterion of Thom and Apelt [9] and the improvement of the Thom and Apelt criterion as used by Burggraf to be bypassed. The study by Runchal, Spalding, and Wofshtein [4] gave numerical results at Reynolds numbers of 1, 10^3, and 10^4 but with a nonuniform mesh size of 13 by 13. These results agree quite well with earlier predictions and with the infinite Reynolds number model proposed by Batchelor.

However, in another study published at about the same time as [4], Runchal and Wolfshtein [11] reported results at a Reynolds number of 10^4 and a uniform mesh spacing of 11 by 11. Thy obtained a primary pair of counterrotating vortices for a square cavity which is a flow field inconsistent with that calculated by the same authors [4] and by Greenspan and proposed by Batchelor.

The contradictions developed by the Imperial College group and the extension of consistent and meaningful converged solutions past a Reynolds number of 400 using an efficient iterative procedure have led the authors to reconsider the cavity-flow problem. We have chosen a recently developed and highly efficient numerical method (see Stone [13]) known as the strongly implicit procedure (SIP) to calculate our solutions.

3. The Governing Equations

The pair of nondimensional differential equations governing the two-dimensional flow are written in terms of the stream function Ψ and the vorticity ω. The differ-

ential equations are the Navier–Stokes equation (in vorticity-transport form) and the equation describing the relationship between Ψ and ω. The latter equation is

$$\omega = -\nabla^2\Psi. \tag{1}$$

The Navier–Stokes equation may be written in either convective form,

$$(1/R)\,\nabla^2\omega - \mathbf{V}\cdot\nabla\omega = 0, \tag{2}$$

or in divergence form.

$$(1/R)\,\nabla^2\omega - \nabla\cdot(\omega\mathbf{V}) = 0. \tag{3}$$

In Eqs. (2) and (3), $\mathbf{V}$ is the velocity vector expressed in terms of Ψ and ∇ is the gradient operator. Equations (2) and (3) are equivalent only for an incompressible fluid. Equations (1) and (2), or Eqs. (1) and (3), represent the system of equations to describe the problem. We have chosen the two different representations in order to determine which description generates the most accurate numerical solution.

The cavity is made nondimensional by scaling with respect to the width of the cavity. The boundary conditions for a square cavity are

$$\begin{aligned}
&\Psi = \partial\Psi/\partial x = 0 && \text{on} \quad x = 0,\ 0 \leqslant y < 1,\\
&\Psi = \partial\Psi/\partial y = 0 && \text{on} \quad y = 0,\ 0 \leqslant x \leqslant 1,\\
&\Psi = \partial\Psi/\partial x = 0 && \text{on} \quad x = 1,\ 0 \leqslant y < 1,\\
&\Psi = 0,\ \partial\Psi/\partial y = -1 && \text{on} \quad y = 1,\ 0 \leqslant x < 1.
\end{aligned} \tag{4}$$

These boundary conditions are the same as those considered by Burggraf [1] and Greenspan [3] and equivalent to those of Pan and Acrivos [2].

The finite-differencing of Eq. (1) and the linear terms in Eqs. (2) and (3) is straightforward. The derivatives at a mesh point are simply replaced by second-order correct central-difference quotients centered about the mesh point. The finite differencing of the nonlinear terms in either Eq. (2) or (3), however, presents greater difficulty. From the many possible schemes for differencing the nonlinear terms, we have selected the following two: (1) central differences using second-order correct difference quotients and (2) unidirectional differences using first-order correct difference quotients which are backward with respect to the local direction of the velocity.

The second-order correct central-difference form of the nonlinear term in Eq. (2) is

$$u_{i,j}\left[\left(\frac{\omega_{i+1,j} - \omega_{i-1,j}}{2h}\right) + O(h^2)\right] + v_{i,j}\left[\left(\frac{\omega_{i,j+1} - \omega_{i,j-1}}{2k}\right)\right] + O(k^2)\Big] \tag{5}$$

where h is the x-direction mesh spacing and k is the y-direction mesh spacing. From Eq. (3), we have

$$\frac{u_{i+1,j}\omega_{i+1,j} - u_{i-1,j}\omega_{i-1,j}}{2h} + O(h^2) + \frac{v_{i,j+1}\omega_{i,j+1} - v_{i,j-1}\omega_{i,j-1}}{2k} + O(k^2), \quad (6)$$

for the second-order correct central-difference representation. In Eqs. (5) and (6), the velocities $u_{i,j}$ and $v_{i,j}$ are given by

$$u_{i,j} = \frac{\Psi_{i,j+1} - \Psi_{i,j-1}}{2k} + O(k^2) \quad (7a)$$

and

$$v_{i,j} = \frac{\Psi_{i-1,j} - \Psi_{i+1,j}}{2h} + O(h^2). \quad (7b)$$

The unidirectional-difference scheme gives rise to difference equations which are quite different in form from the central-difference representation. From Eq. (2), we have

$$u_{i,j}\left[\frac{A_1\omega_{i+1,j} + A_2\omega_{i,j} + A_3\omega_{i-1,j}}{h} + O(h)\right] + v_{i,j}\left[\frac{A_4\omega_{i,j+1} + A_5\omega_{i,j} + A_6\omega_{i,j-1}}{k} + O(k)\right] \quad (8)$$

for the nonlinear term. The divergence form from Eq. (3) gives rise to the nonlinear term,

$$\frac{A_1(u\omega)_{i+1,j} + A_2(u\omega)_{i,j} + A_3(u\omega)_{i-1,j}}{h} + O(h) + \frac{A_4(v\omega)_{i,j+1} + A_5(v\omega)_{i,j} + A_6(v\omega)_{i,j-1}}{k} + O(k). \quad (9)$$

In Eqs. (8) and (9), we have

$$\begin{aligned} &A_1 = +1, \quad A_2 = -1, \quad A_3 = 0 \quad \text{when} \quad u_{i,j} < 0, \\ &A_1 = 0, \quad A_2 = +1, \quad A_3 = -1 \quad \text{when} \quad u_{i,j} \geqslant 0, \\ &A_4 = +1, \quad A_5 = -1, \quad A_6 = 0 \quad \text{when} \quad v_{i,j} < 0, \\ \text{and} \quad &A_4 = 0, \quad A_5 = +1, \quad A_6 = -1 \quad \text{when} \quad v_{i,j} \geqslant 0. \end{aligned} \quad (10)$$

In Eqs. (5)–(9), the term reading $0(h^n)$ indicates an error term of order h to the nth power.

Although the two differential forms of the vorticity-transport equation are equivalent, their finite-difference forms are quite different. The difference equations for the convective form of the vorticity-transport equation contain product terms in which the velocity and vorticity are evaluated at different points. In the divergence form, the velocity–vorticity products are evaluated at the same point.

Thus, there are four possibilities in representing the nonlinear terms of the Navier–Stokes equation in difference form. They are (1) central differences on the convective form (CDC), central differences on the divergence form (CDD), unidirectional differences on the convective form (UDC), and unidirectional differences on the divergence form (UDD). Each of these four possibilities will be considered in order to determine the optimum representation for the problem.

The boundary conditions given in Eq. (4) are suficient for the analytical solution of the boundary-value problem. However, numerical methods require the specification of boundary conditions for each of the dependent variables. Therefore, the vorticity at the wall is given in terms of the normal variation of the tangential velocity since the normal velocity is always zero for an impervious wall with zero normal velocity,

$$\omega_w = (\partial v_t/\partial l_n)_w\,, \tag{11}$$

where v_t = tangential velocity, and l_n = normal length coordinate, and w denotes wall. In terms of the stream function, Eq. (11) is written as

$$\omega_w = (\partial^2\psi/\partial l_n{}^2)_w\,. \tag{12}$$

Equation (12) is expressed in terms of a Taylor series evaluated at the first interior mesh point. This procedure gives the following as a set of third-order correct boundary conditions:

$$\begin{aligned}
\omega_{i,1} &= \frac{-3\psi_{i,2}}{k^2} - \frac{\omega_{i,2}}{2} && (i = 2, 3,..., I \quad \text{on} \quad y = 0, 0 < x < 1),\\
\omega_{I+1,j} &= \frac{-3\psi_{I,j}}{h^2} - \frac{\omega_{I,j}}{2} && (j = 2, 3,..., J \quad \text{on} \quad x = 1, 0 < y < 1),\\
\omega_{i,J+1} &= \frac{-3\psi_{i,J}}{k^2} - \frac{\omega_{i,J}}{2} - \frac{3}{k^2} && (i = 2, 3,..., I \quad \text{on} \quad y = 0, 0 < x < 1),\\
\omega_{1,j} &= \frac{-3\psi_{2,j}}{h^2} - \frac{\omega_{2,j}}{2} && (j = 2, 3,..., J \quad \text{on} \quad x = 0, 0 < y < 1).
\end{aligned} \tag{13}$$

Third-order correct boundary conditions were preferred because of the increased accuracy obtained over the typical first-order correct boundary conditions. When convergence problems were encountered in a solution sequence, first-order

boundary conditions were examined to determine if a converged solution was obtainable at a lower order of error.

From Eq. (13), we see that the vorticity at the cavity corners has not been specified. It follows from Eq. (11) that the vorticity, at points (x, y) equal (0, 0) and (1, 0), has the value zero. The points (x, y) equal (1, 1) and (0, 1) are singular and the vorticity there is undefined. However, this dilemma does not affect the improvement of the dependent variables at interior mesh points.

Previous numerical investigations [7, 9, 11] have shown that, if the new wall vorticity values, computed from the latest set of stream-function values, are used directly to compute new vorticity values in the interior, the computational procedure will not converge. An effective procedure for stabilizing the computations is to weight-average the new and old wall-vorticity values. Thus, the "new" wall-vorticity value used in the next iteration is defined by

$$\omega_{i,j}^{n+1})_w = (1 - \gamma)\, \omega_{i,j}^{n})_w + \gamma \omega_{i,j}^{*})_w\,, \tag{14}$$

where γ = wall-vorticity weight-averaging coefficient (determined by numerical numerical experimentation). $\omega_{i,j}^{*})_w$ = wall-vorticity value computed from the improved ψ values, $\omega_{i,j}^{n})_w$ = vorticity boundary value from the previous iteration, and $\omega_{i,j}^{n+1})$ = new vorticity boundary value used in the iterative improvement of the vorticity solution values at interior mesh points. Values of γ were found to range from 0.4 to 0.6 with 0.6 being best.

We have considered the cavity problem using the idea of an iterative numerical method developed by Stone [13] and known as the strongly implicit procedure (SIP). The SIP method is a procedure designed to reduce the computational effort required to solve the large sets of algebraic equations arising from the approximation of a set of elliptic, multidimensional partial differential equations. The method is based on an inexact triangular decomposition of the coefficient matrix. Stone showed that the SIP method was three to five times more efficient than the alterating direction implicit (ADI) method for several model problems. Birkhoff, Varga, and Young [14] have also shown that ADI is approximately four times as efficient as the extrapolated Liebmann method for small mesh sizes.

4. Results

In order to evaluate the difference schemes mentioned in the previous section, we have considered solutions to the cavity-flow problem for a range of Reynolds numbers. The convergence criterion used pertained to minimization of each mesh-point residual r for each difference equation. The residual minimization, while not exact, is an accurate criterion for solution as long as the coefficient matrix of the difference equation is not a nearly singular matrix.

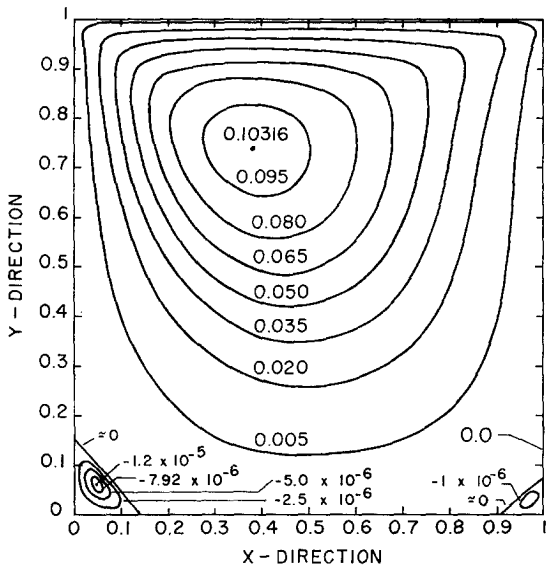

FIG. 1. Streamline patterns and stream function values for flow in a square cavity, $R = 100$, $h = 1/50$, CDD.

TABLE I

Percent Difference in Stream Function Values at the Midpoint Relative to the CDD Solution Value for Grid Size 1/50. ($R = 100$, max $| r_{i,j} | \leqslant 0.25 \times 10^{-4}$).

Difference scheme	Relative difference (%)			
	21 × 21 grid	31 × 31 grid	41 × 41 grid	51 × 51 grid
CDC	11.12	4.78	2.55	1.51
CDD	2.06	0.648	0.206	0.000
UDC	10.92	6.48	4.46	3.34
UDD	13.81	11.20	9.20	7.70

For $R = 10$, we found that all four of the differencing schemes yielded converged solutions for mesh spacings of 1/20, 1/30, 1/40, and 1/50. The CDD procedure generated solution values which were closer to the apparent limiting values at lower iteration counts than did the other three methods. The convergence criterion was $r_{\max} \leqslant 10^{-4}$. However, the superiority of the CDD procedure over the other

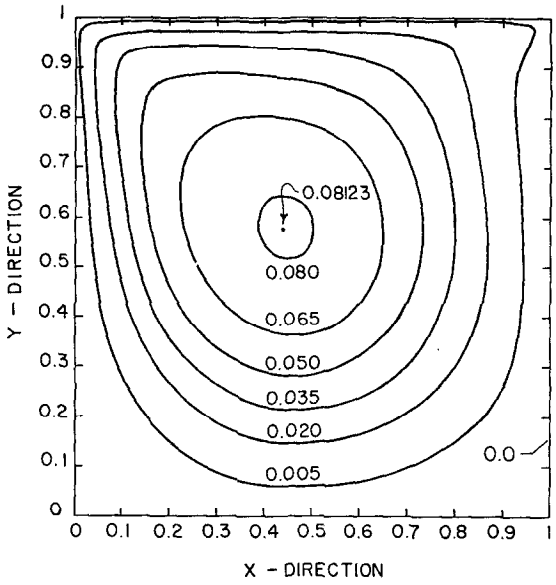

FIG. 2. Streamline pattern and stream function values for flow in a square cavity, $R = 1000$, $h = 1/50$, UDD.

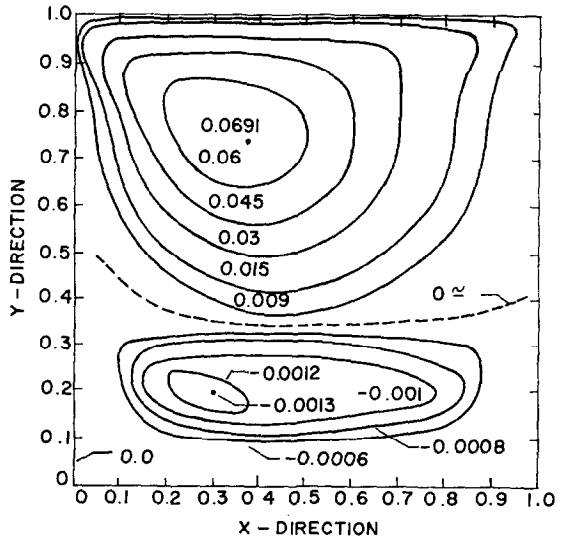

FIG. 3. Streamline pattern and stream function values for flow in a square cavity, $R = 1000$, $h = 1/30$, UDC.

three procedures is not clearly demonstrated at $R = 10$. At a Reynolds number of 100, the superiority of the CDD procedure was clearly exhibited. The convergence to the apparent limiting value was much more rapid with decreasing mesh size for the CDD procedure. Figure 1 shows the streamline plot at $R = 100$ for the CDD method at a mesh spacing of 1/50. This plot shows the trend toward agreement with Batchelor's model. If the CDD solution at a mesh spacing of 1/50 is taken as the reference point, a comparison may be made of both differencing procedure and mesh size. This comparison is shown in Table I for the midpoint of the square cavity. Notice how close the 1/20-spacing solution is to the 1/50-spacing solution. The superiority of the CDD method is actually expected because it is the only one of the four methods which conserves vorticity in a local sense [16].

The next Reynolds number for which solutions were attempted was 1000. Both central-difference procedures failed to converge at this Reynolds number while both unidirectional-difference methods did satisfy the specified convergence criteria. The solutions obtained using the UDD method for mesh spacings of 1/20 and 1/50 were consistent with Batchelor's model while the UDC solution differed from the expected solution. The UDD solution is shown in Fig. 2 for $h = 1/50$ while the UDC solution is depicted in Fig. 3 for a mesh spacing of 1/30. (The same form of result was obtained for UDC at $h = 1/20$.)

The UDD solution in Fig. 2, besides being consistent with Batchelor's model, is similar in form to that obtained by Greenspan [3], by Runchal, Spalding, and Wolfshstein [4], by Gosman *et al.* [12], and by Torrance *et al.* [15]. The UDC solution (Fig. 3) obtained here is inconsistent with what is expected from Batchelor's model and from the other cited investigations because there are two large vortices instead of one occupying the square cavity.

We attribute the difference between Fig. 2 and 3 to be based on the different finite-difference representations. The discrepancy indicates that the UDC method differencing does not yield adequate results at a mesh spacing of 1/30 and a Reynolds number of 1000. This difference in the form of the vortex pattern implies that extreme care should be exercised in the selection of the form of the governing differential equations and their finite-difference representation. The work of other investigators was done using either CDC or UDC procedures or a hybrid UDC–UDD method. (Runchal *et al.* [4] and Gosman *et al.* [12] did not actually use UDC but used a hybrid form of UDD and UDC.) The CDC calculations were restricted to Reynolds numbers of 400 or less. The UDC procedure was used by others when large Reynolds number calculations were desired. The Runchal–Wolfshtein study [11] used a mesh spacing of 1/10 with the UDC method to get a result similar to Fig. 3 for a Reynolds number of 10,000. Since this type of result is invalid, it appears that a mesh size of 1/10 is too coarse for $R = 10{,}000$ in the hybrid method.

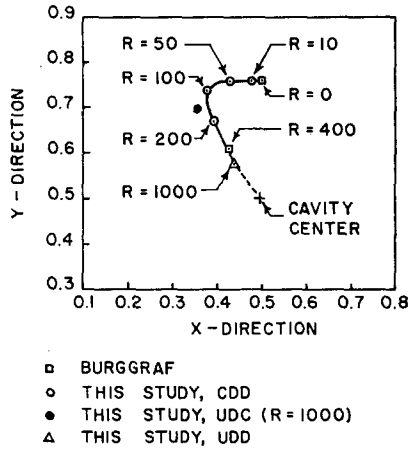

FIG. 4. Effect of Reynolds number on the location of the center of the primary vortex, CDD and UDD method.

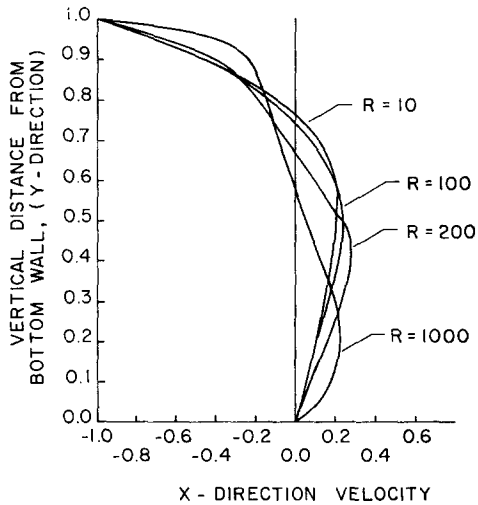

FIG. 5. Velocity traverse along a vertical line through the vortex center.

Figure 4 shows how the vortex center behaves as a function of Reynolds number. Note that the vortex center is moving toward the cavity center as the Reynolds number increases. This behavior is consistent with the Batchelor model for large Reynolds numbers. Figure 4 also shows a calculation at a Reynolds number of 200 which was sought in order to have a more complete numerical description

of the flow field. The point indicated by the solid circle in Fig. 4 shows the UDC value at a Reynolds number of 1000. This point further indicates the deviation of the UDC solution from the trend suggested by Batchelor.

Figure 5 shows the velocity traverse through the vertical center-line of the cavity for different Reynolds numbers. Calculations for the largest Reynolds number show that a constant vorticity core is developing (as predicted by Batchelor).

Convergence was not attained at Reynolds numbers higher than 1000 for the unidirectional methods. However, other studies reported converged results at Reynolds numbers significantly above 1000. Greenspan [3, 10], Runchal *et al.* [4], Gosman *et al.* [12] all obtained solutions at a Reynolds number of 10,000 using either the UDC or hybird method. As already stated, the Greenspan results follow the expected trend; however, the convergence criteria is felt to be inadequate for accurate solutions. Greenspan also did not show the corner vortices which should have been detectable using his procedure.

The results presented thus far in this study are felt to be closer to the exact numerical solution than those of [4] and [12] because of the convergence criteria employed herein. Our convergence criteria are based on residual minimization at each mesh point while the studies of [4] and [12] are based on finding values of Ψ and ω such that $(\Psi^{(n+1)} - \Psi^{(n)})/\Psi^{n+1} \leqslant \epsilon$. The idea of residual minimization is to take the algebraic difference equations in the form

$$A\mathbf{x} = \mathbf{b}$$

and define the residual as

$$\mathbf{r} = A\mathbf{x} - \mathbf{b}.$$

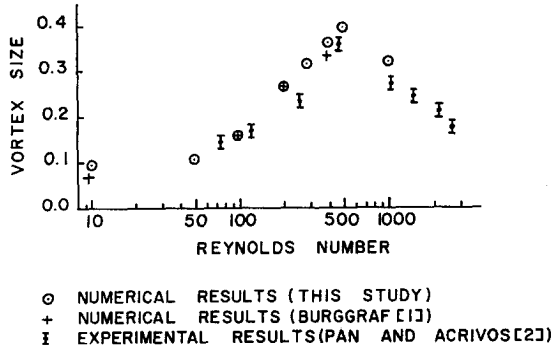

FIG. 6. Variation in the size of the upstream corner vortex with Reynolds number for a square cavity.

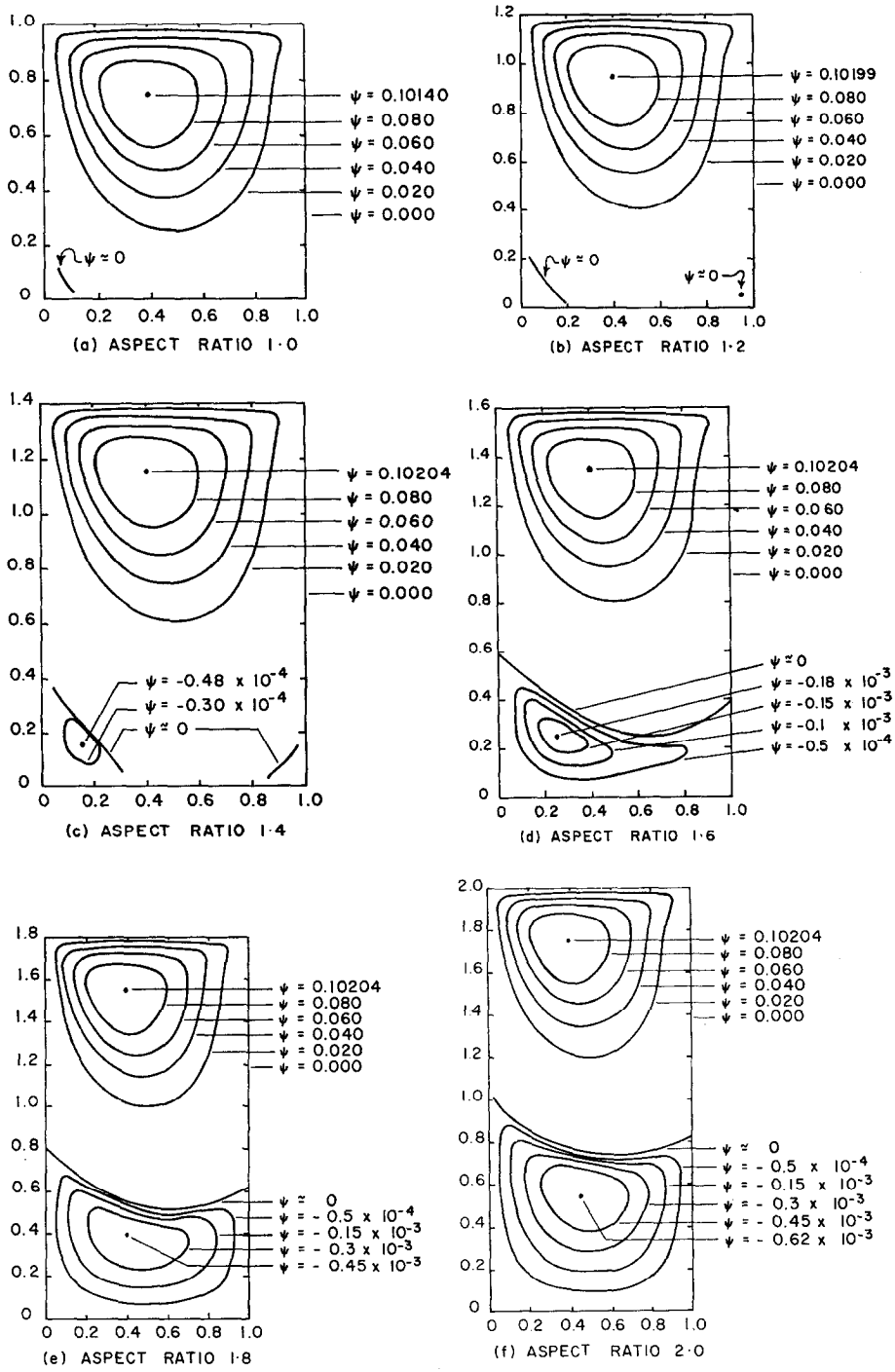

FIG. 7. Effect of aspect ratio on vortex size and strength at $R = 100$.

The residual at each mesh point is examined during the iterative process and when the maximum residual value is less than a prescribed small quantity (10^{-4} for this study), we say that the numerical solution has converged. We feel that this residual minimization technique is superior to the method of relative differences in the stream function as used by [4] and [12]. The stream-function criterion is subject to a scaling problem in the vicinity of very small values of Ψ. Furthermore, the type of numerical technique used in this approach has been shown [13] to be vastly superior to the Gauss–Seidel method used in [4] and [12].

Figure 6 shows the variation in size of the upstream corner vortex with increasing Reynolds number The numerical results of Burggraf [1] and experimental results of Pan and Acrivos [2] are shown for comparison. Note the consistency of the numerical results with observations for Reynolds number greater than 500.

Figure 7 shows the formation of the secondary vortex as the cavity depth increases These calculations were done for the CDD method at a Reynolds number of 100 and a mesh spacing of 1/20. As the cavity depth increases from 1 to 2, the corner vortices grow in size, but remain relatively weak, and occupy the entire lower portion stream-function value does not change as the cavity depth continues to increase.

5. Conclusions

We have performed a systematic evaluation of four different methods of finite-differencing the Navier–Stokes equations. The numerical scheme used was the SIP method and was the same for each differencing method.

The results obtained agree quite closely with those obtained by other investigators considering this same problem. The results indicate that, for a square mesh and Reynolds numbers of 100 and below, the CDD method generated the most accurate solutions. At a Reynolds number of 1000 for a square mesh, the UDD solution converged to a physically consistent solution while the UDC solution converged to an unrealistic solution. The UDC solution shows the affect that the form of the governing differential equations has on the numerical answer.

The vortex formation for a cavity of increasing depth was calculated using the CDD method at a Reynolds number of 100. This set of calculations illustrate vividly how the corner vortices change when the cavity aspect ratio changes.

We feel that, based on the systematic study of different differencing methods, an efficient iterative scheme, and the convergence criteria, the results presented here are the best numerical solutions presently available for the problem of a recirculating flow in a cavity.

ACKNOWLEDGMENTS

JDB acknowledges the fellowship support of the National Science Foundation and the Resident Assistantship program at NASA-MSC. We thank Herb Stone and Herb Weinstein of Esso Production Research Company for several helpful discussions.

REFERENCES

1. O. BURGGRAF, Analytical and numerical studies of the structure of steady separated flows, *J. Fluid Mech.* **24** (1966), 113–151.
2. F. PAN AND A. ACRIVOS, Steady flows in rectangular cavities, *J. Fluid Mech.* **28** (1967), 643–655.
3. D. GREENSPAN, Numerical studies of prototype cavity flow problems, *Comput. J.* **12** (1969), 89–94.
4. A. K. RUNCHAL, D. B. SPALDING, AND M. WOLFSHTEIN, Numerical solution of the elliptic equations for transport of vorticity, heat, and matter in two-dimensional flow, *Phys. Fluid.* **12** (1969), II-21–II-28.
5. M. KAWAGUTI, Numerical solution of the Navier-Stokes equations for the flow in a two-dimensional cavity, *J. Phys. Soc. Japan*, **16** (1961), 2307–2315.
6. G. K. BATCHELOR, On steady laminar flow with closed streamlines at large Reynolds numbers, *J. Fluid Mech.*, **1** (1956), 177–190.
7. R. D. MILLS, Numerical solutions of the viscous flow equations for a class of closed flows, *J. Roy. Aero. Soc.*, **69** (1965), 714–718.
8. H. K. MOFFATT, Viscous and resistive eddies near a sharp corner, *J. Fluid Mech.* **18** (1964), 1–18.
9. A. THOM AND C. J. APELT, "Field Computations in Engineering and Physics," Van Nostrand, London, 1961.
10. D. GREENSPAN, "Lectures on the Numerical Solution of Linear, Singular, and Nonlinear Differential Equations," Prentice Hall, New York, 1968.
11. A. K. RUNCHAL AND M. WOLFSHTEIN, Numerical integration procedure for the steady state Navier–Stokes equations, *J. M. E. Sci.* **11** (1969), 445–453.
12. A. D. GOSMAN, W. M. PAN, A. K. RUNCHAL, D. B. SPALDING, AND M. WOLFSHTEIN, "Heat and Mass Transfer in Recirculating flows," Academic Press, New York, 1969.
13. H. L. STONE, Iterative solution of implicit approximations of multidimensional partial differential equations, *SIAM J. Num. Anal.*, **5** (1968), 530–558.
14. G. BIRKHOFF, R. S. VARGA, AND D. M. YOUNG, Alternating direction implicit methods, *in* "Advances in Computers," (F. L. Alt and M. Rubinoff, Eds.), Vol. 3, 189–273, Academic Press, New York, 1962.
15. K. TORRANCE, R. DAVIS, K. EIKE, P. GILL, D. GUTMAN, A. HSUI, S. LYONS, AND H. ZIEN, Cavity flows driven by buoyancy and shear, *J. Fluid Mech.*, **51** (1972), 221–231.
16. R. D. RICHTMYER AND K. W. MORTON, "Difference Methods for Initial-value Problems," 2nd Ed., Interscience Publishers, New York, 300.